Warming and lateral shift of the Gulf Stream from in situ observations since 2001

Robert E. Todd[1*] and Alice S. Ren[1]

[1*]Physical Oceanography Department, Woods Hole Oceanographic Institution, 266 Woods Hole Rd., MS#21, Woods Hole, 02543, MA, USA.

*Corresponding author(s). E-mail(s): rtodd@whoi.edu; Contributing authors: alice.ren@whoi.edu;

Abstract

As the poleward flowing western boundary current of the North Atlantic ocean, the Gulf Stream plays a key role in the climate system. Here we show that from 2001 to 2023 the Gulf Stream west of 68°W has experienced both surface-intensified warming due to heat uptake at a rate exceeding the global average and a bulk lateral shift towards its cooler shoreward side at a rate of about 5±2 km per decade. The Gulf Stream west of 68°W now has an O(10)-m-thick surface layer of warmer (by ∼1 °C) and lighter (by ∼0.3 kg m^{-3}) water, contributing to increased upper ocean stratification. Our results rely on over 25,000 temperature and salinity profiles collected by autonomous profiling floats and underwater gliders in the region, allowing robust estimation of trends and clear attribution of observed changes to both ocean heat uptake and a lateral shift of the Gulf Stream.

The Gulf Stream is a key oceanic component of the Earth's climate system [1, 2], transporting heat [3] and nutrients [4] from the tropics to subpolar latitudes in its dual role as the western boundary current of the wind-driven

North Atlantic subtropical gyre [5] and as part of the buoyancy-driven Atlantic Meridional Overturning Circulation (AMOC) [6]. As the climate warms, western boundary currents are expected to shift poleward [7], potentially driving localized acceleration of ocean warming [8, 9], shifts in faunal boundaries [10, 11], and influencing the atmospheric storm track [2, 12].

The Gulf Stream is characterized by large cross-frontal gradients of temperature, salinity, and density and an associated frontal jet [13–15]. Throughout its course, the Gulf Stream meanders about its mean position with the largest meanders occurring north and east of Cape Hatteras, NC after the current separates from the continental margin. At a fixed location, these meanders cause large variability in water properties on time scales of days to weeks [16, 17], despite the relatively invariant cross-stream structure of the Gulf Stream [13, 18]. This large intrinsic Gulf Stream variability makes detection and attribution of long-term changes in Gulf Stream properties difficult [19]. Regionally accelerated near-surface warming has been documented in the Gulf Stream [8], and some analyses have shown evidence of a poleward shift in its path [19–23] as predicted by climate simulations [9]. Other analyses have found equatorward shifts in Gulf Stream position, particularly east of 65°W [24, 25]. Due to differences in location, time span, and methodology, these results are not necessarily contradictory, but rather indicate the complex variability in the system.

Since the turn of the 21st century, the Argo program has revolutionized oceanography by providing routine measurements of upper ocean temperature and salinity throughout the ice-free ocean basins [26]. Although of great value, the nominal horizontal and temporal spacing between Argo profiles of 300 km and 10 days limits the ability of Argo observations to capture the mean and annual cycle in the vicinity of narrow, strongly varying features like the Gulf Stream using these data [27]. For this reason, our group has used Spray underwater gliders [28] to collect dense observations within and near the Gulf Stream between southern Florida and New England since 2015 [29, 30] (Fig. 1b). The set of glider-based observations now amassed allows us to construct three-dimensional estimates of the time mean and annual cycle of Gulf Stream water properties for the base period from July 2015 to May 2023 (e.g., Fig. 1a; see Online Methods for details).

For the Gulf Stream region along the US East Coast where we can make reliable estimates of the mean and annual cycles of temperature, salinity, and potential density, Argo floats provide 4,335 profiles spanning from 4 June 2001 to 1 July 2023; gliders provide 20,993 profiles through 11 April 2023, most of which were collected since 2015 (Fig. 1). We treat the Argo and glider profiles as a unified set of observations spanning more than 20 years and covering the Gulf Stream from the Florida Strait near 26°N, 79°W to approximately 38°N, 68°W (which is roughly 600 km downstream from Cape Hatteras, NC).

Observed temperature, salinity, and density trends

For each Argo and glider profile in our combined data set, we compute anomalies relative to the three-dimensional annual cycle (see Online Methods), which results in removal of 80% or more of temperature variance at each depth level down to 890 m and more than 65% of salinity and potential density variance shallower than 700 m, by which depth salinity and density variance has fallen by about an order of magnitude compared to the near-surface. This removal of seasonal and spatial variability allows us to combine observations spread over the Gulf Stream region to evaluate temporal trends. For example, Fig. 2 shows a statistically significant temperature increase of $0.06 \pm 0.02\,^{\circ}\mathrm{C\,yr^{-1}}$ at a depth of 200 m. Unsurprisingly, annually averaged anomalies show interannual variability about the fitted trend (Fig. 2, black).

Throughout the upper 890 m of the water column, there is a statistically significant warming trend for the Gulf Stream region since 2001 (Fig. 3a, blue). This warming is associated with decreasing density (Fig. 3c, blue), except possibly deeper than 500 m, as the observed trend toward increasing salinity at depths below 60 m (Fig. 3b, blue) does not fully compensate for the effect of the temperature trend on density. With a more strongly negative density trend at shallower depths compared to deeper depths (Fig. 3c, blue), upper ocean stratification has been increasing in the Gulf Stream region since 2001. Our finding of a warming trend of about 0.05–0.07 °C yr^{-1} in the upper 250 m (Fig. 3a, blue) agrees well with regional trends reported from longer term records of satellite-derived sea surface temperature in the Gulf Stream [20] and is slightly higher than the 0.037 ± 0.006 and 0.039 ± 0.006 °C yr^{-1} sea surface temperature trends reported for the Middle Atlantic Bight continental shelf and slope to the west of the Gulf Stream during 1982–2018 [31]. All of these regional warming rates are markedly larger than the 0.005 °C yr^{-1} globally averaged trend in the upper 500 m from Argo profiles during 2006–2013 [32], confirming previous reports of enhanced warming in the northwestern subtropical Atlantic [8]. In recent years, adjacent coastal waters have been warming even faster, with rates of 0.11 ± 0.02 °C yr^{-1} over the Middle Atlantic Bight continental shelf during 2002–2013 [33] and 0.23 °C yr^{-1} in the Gulf of Maine during 2004–2013 [11].

Causes of observed trends

Temperature and salinity changes at fixed points in space result from the combination of temporal changes in water mass properties and spatial shifting of water property gradients. With concurrent profiles of temperature, salinity, and density available from gliders and floats, we are able to disentangle these two effects in the Gulf Stream region.

Changes in water mass properties manifest as density-compensated changes in temperature and salinity on isopycnal surfaces. Near the sea surface, along-isopycnal increases in temperature (Fig. 3a, red) account for about half of the total observed warming trend (Fig. 3a, blue). This signal of water mass property change decays with depth, falling to zero near a depth of 200 m (Fig. 3a, red). The compensating increase in salinity along isopycnals (Fig. 3b, red) is over 0.01 salinity units per year in the upper 70 m, a depth range with weak total salinity trend (Fig. 3b, blue). At depths of 220–500 m, water mass property trends are generally insignificant (Figs. 3a–b, red). Below this there is a trend toward warmer and saltier water, which may reflect previously noted decadal-scale changes in waters that are ventilated in the Labrador Sea and carried southward in the Deep Western Boundary Current (DWBC) [34].

We can diagnose the rate of heat gain within the Gulf Stream from along-isopycnal temperature trends (see Online Methods). In a regional domain with open boundaries as considered here, it is important to exclude temperature trends due to shifting property gradients, which would average out in a global- or basin-scale calculation. Over the upper 200 m, the rate of heat gain for the Gulf Stream region shown in Fig. 1 is 0.6±0.4 W m^{-2} during 2001–2023. Over the upper 890 m, the rate increases to 1.1±0.6 W m^{-2}. For comparison, global estimates of heat gain from Argo observations are 0.4 to 0.6 W m^{-2} over the upper 2000 m during 2006–2013 [32] and 0.61±0.09 W m^{-2} for the upper 1800 m during 2005–2015 [35]. For the period 1955–2010 the upper 700 m of the global ocean gained heat at a rate of 0.27 W m^{-2} [36]. Rates of heat uptake in the Gulf Stream west of 68°W rival or exceed those of the global ocean over substantially greater vertical extent during overlapping time periods, implying that the Gulf Stream has gained heat more rapidly than the global ocean during 2001–2023.

By construction, the along-isopycnal trends in temperature and salinity (Figs. 3a–b, red) do not contribute to changes in density (Fig. 3c, red). Residual non-isopycnal trends in temperature and salinity (Figs. 3d–e, green) and the potential density trend (Fig. 3c, blue) result from shifts in lateral and vertical property gradients. The Gulf Stream front generally separates warmer, saltier, and lighter waters on its offshore or equatorward side from colder, fresher, and denser waters on the shoreward or poleward side [15], so the signs of our non-isopcynal temperature and salinity trends (Figs. 3a–b, red) and density trend (Figs. 3c, blue) suggest a shift of the Gulf Stream towards its colder side. With quantitative estimates of the cross-stream and vertical gradients that typify the Gulf Stream front from glider observations, we can estimate the bulk long-term motion of the Gulf Stream required to account for the non-isopycnal trends in Fig. 3 (see Online Methods). We find that the Gulf Stream's frontal structure has shifted towards its colder side at a rate of 0.5 ± 0.2 km yr^{-1} and deepened at a rate of 0.8 ± 0.5 m yr^{-1} over the period 2001–2023.

Discussion

The inferred downward shift in Gulf Stream frontal structure can be interpreted as the near-surface manifestation of the surface-intensified heat gain detected on isopycnal surfaces (Figs. 3a, red); a warming trend will generally cause surface waters to become less dense, depressing isopycnal surfaces. We note that the total salinity trend in the upper 60 m is not significantly different from zero (Fig. 3b, blue), consistent with the surface ocean gaining heat from the atmosphere without significant changes in net evaporation and precipitation. Compared to the turn of the 21st century, the Gulf Stream region now has an O(10)-m-thick surface layer of warmer (by about 1 °C) and lighter (by about 0.3 kg m^{-3}) water, which contributes to the overall increase in upper ocean stratification. This increasing stratification tends to inhibit vertical exchanges of heat, carbon, and nutrients between the surface mixed layer and the interior ocean [37–39] and impacts the general ocean circulation through changes in the characteristic scales and propagation speeds of eddies, fronts, and other baroclinic features [39].

The inferred lateral shift in the Gulf Stream of 5±2 km per decade since 2001 is in the same direction as and about half the magnitude of the shift found in a global climate model with doubling of atmospheric carbon dioxide [7]. Generally, climate simulations predict an expansion of the subtropical gyres and poleward shifting of the mid-latitude western boundary currents due to poleward shifts in the atmospheric circulation [7, 20]. In the North Atlantic, projected reduction in DWBC transport as part of a slowing AMOC may additionally contribute to a poleward shift in the latitude at which the Gulf Stream leaves the continental margin [21]. The rate of translation inferred here is small enough that it has been challenging to measure directly via satellite-based remote sensing due to the large amplitude of Gulf Stream meanders [17, 40–42] and the relatively coarse (O(10) km along track) resolution of measurements.

This slow lateral translation implies that the Gulf Stream is roughly 10 km closer to the edge of the continental shelf along the US East Coast than it was at the turn of the 21st century, which may be a contributing factor [43] in the accelerated warming over the Middle Atlantic Bight continental shelf and slope [33, 44] and in the Gulf of Maine [11]. This shift in Gulf Stream position may affect ecosystems by shifting the boundary between distinct pelagic populations [10] and by changing conditions in adjacent coastal waters [11]. Given that air-sea heat and moisture fluxes from western boundary currents set the latitude of the mid-latitude storm track [2], the lateral shift in the Gulf Stream is likely to impact atmospheric circulation in complex ways [45, 46].

Our inferred cross-stream and vertical shifts in the Gulf Stream front do not account for all of the observed non-isopycnal changes in temperature, salinity, and density. Trends reconstructed from observed, stream-coordinate gradients and inferred motion (Fig. 3c–e, magenta with the fraction of trend captured across depths shown as a percentage) differ most from the observed trends (Figs. 3d–e, green and Fig. 3c, blue) in the upper 100 m of the water column, where a non-isopycnal freshening trend intensifies the near-surface density trend. These residuals are likely the result of changes to the temperature, salinity, and density gradient fields and/or spatial variability in the motion of the Gulf Stream front that are not captured by our analysis of the bulk movement of the Gulf Stream front. Changes to the structure of the Gulf Stream would be tied to changes in the velocity field since the Gulf Stream is largely in geostrophic or gradient wind balance [47]. Glider-based current profiles in the Gulf Stream are available since July 2015 [29]; as the velocity record length grows, such changes to currents should be detectable. That will allow us to examine how upper ocean heat transport in the Gulf Stream may be changing as the ocean continues to gain heat in the warming climate.

In this analysis, we have been able to clearly identify trends in Gulf Stream temperature, salinity, and density along the US East Coast since 2001. Critically, we can attribute those changes to a combination of surface-intensified water property changes as the ocean takes up additional heat and a lateral shift of the Gulf Stream towards its colder (i.e., shoreward or poleward) side at a rate of approximately 5 km per decade. The sustained, high-resolution observations from underwater gliders since 2015 uniquely allow for estimation of three-dimensional annual cycles for the Gulf Stream region. This in turn enables us to compute temperature, salinity, and density anomalies from more than 25,000 Argo and glider profiles spanning more than 20 years in the Gulf Stream region and to estimate multi-decadal trends with high statistical confidence. The concurrent measurements of temperature and salinity throughout the water column are key to clearly attributing observed trends to specific physical mechanisms. These results highlight the crucial and ongoing role of autonomous profiling platforms in providing the long-term ocean observations that capture changes in the Earth's climate system.

Acknowledgments. Spray glider operations in the Gulf Stream have relied on P. Deane at the Woods Hole Oceanographic Institution (WHOI) and the Instrument Development Group at the Scripps Institution of Oceanography. Glider-based surveys have been supported by the National Science Foundation (awards OCE-0220769 to W.B. Owens; OCE-0220930 to R.E. Davis; OCE-1558521, OCE-1633911, and OCE-1923362), the Office of Naval Research (awards N00014-17-1-3040, N00014-17-1-2968, N00014-18-1-2425, N00014-21-1-2294), the NOAA Global Ocean Monitoring and Observing Program (awards NA14OAR4320158 and NA19OAR4320074, doi: 10.13039/100018302), WHOI, and Eastman, all to RET except as noted. ASR was supported by the Postdoctoral Scholar Program at WHOI, with funding provided by the Doherty Foundation. The importance of the long-term efforts of the global Argo program cannot be understated.

Author Contributions Statement. RET conceived of the idea to analyze long-term trends in the data and led the glider data collection efforts. RET and ASR developed and conducted the analysis methods. RET wrote the manuscript. RET and ASR edited the manuscript.

Competing Interests Statement. The authors declare no competing interests.

1 Figures

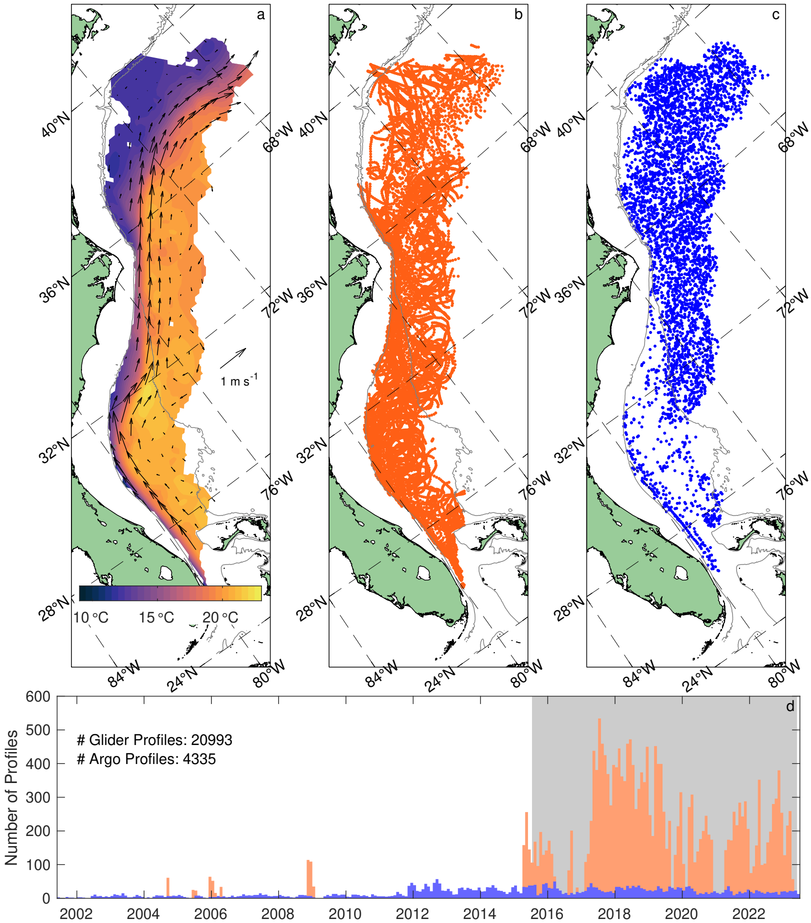

Fig. 1 Gulf Stream observations used here. (a) Mean potential temperature (color) and velocity (vectors) at 200 m for the Gulf Stream region based on glider observations from 2015–2023. (b–c) Locations of individual profiles from (b) Spray gliders and (c) Argo floats during 2001–2023 that are used for analysis of long-term trends. (d) Monthly distribution of profiles from gliders (orange) and Argo floats (blue) with grey shading indicating the period used to estimate the mean and annual cycle from glider observations as in (a).

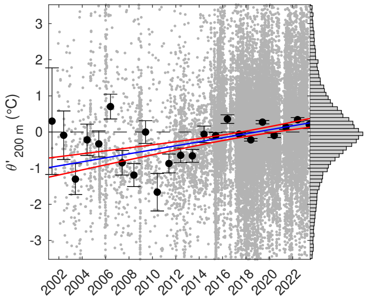

Fig. 2 Example of observed trend in potential temperature. Grey dots are potential temperature anomalies (θ') from glider and Argo measurements at a depth of 200 m relative to the period 2015–2023. For presentation purposes only, the largest 5% of anomalies (magnitudes greater than 3.5 °C) are omitted; the histogram along the right-hand axis indicates the distribution of anomalies across all years. The blue line is the fitted trend with the 95% confidence interval about the trend indicated in red. Black dots and whiskers denote the 95% confidence interval for the mean temperature anomaly in each calendar year.

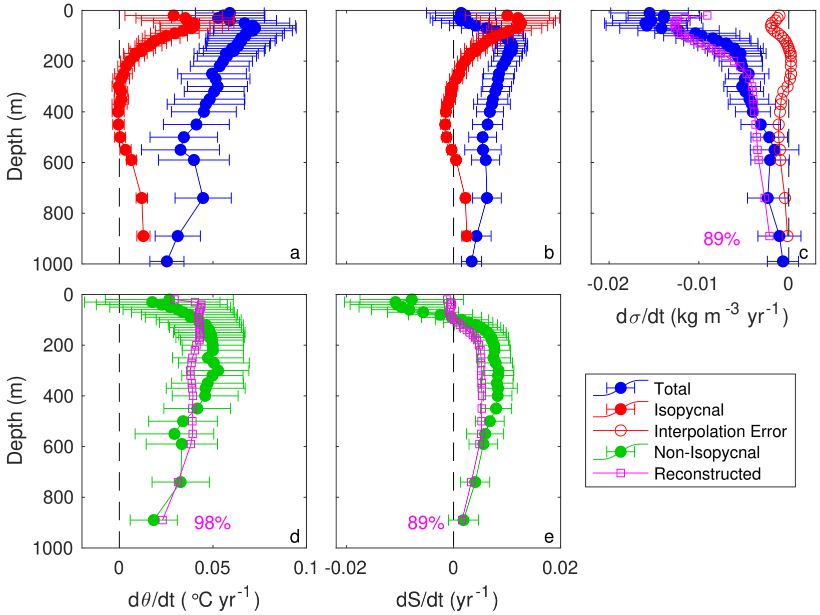

Fig. 3 Vertical profiles of trends in Gulf Stream properties. (a,d) Potential temperature, (b,e) salinity, and (c) potential density. In (a–c), total observed trends are blue. In (a–b), temperature and salinity trends relative to isopycnal surfaces are red; in (c) the degree to which the isopycnal temperature and salinity trends in (a–b) are uncompensated due to interpolation errors in shown by open red markers. In (d–e), the non-isopycnal temperature and salinity trends resulting from shifting property gradients are green. Trends reconstructed from inferred translation of the mean cross-stream and vertical temperature, salinity, and density gradients are shown by open magenta boxes in (d), (e), and (c), respectively. Magenta percentages in (c–e) indicate the fraction of the mean-square trend captured by the reconstructed trends. For all observed trends, whiskers indicate the 95% confidence interval for the trend at each depth.

References

[1] Minobe, S., Kuwano-Yoshida, A., Komori, N., Xie, S.-P. & Small, R. J. Influence of the Gulf Stream on the troposphere. *Nature* **452**, 206–209 (2008). https://doi.org/10.1038/nature06690 .

[2] Kwon, Y.-O. *et al.* Role of the Gulf Stream and Kuroshio–Oyashio systems in large-scale atmosphere-ocean interaction: A review. *J. Climate* **23** (12), 3249–3281 (2010). https://doi.org/10.1175/2010JCLI3343.1 .

[3] Palter, J. B. The role of the Gulf Stream in European climate. *Annu. Rev. Mar. Sci.* **7**, 113–137 (2015). https://doi.org/10.1146/annurev-marine-010814-015656 .

[4] Whitt, D. B. *On the role of the Gulf Stream in the changing Atlantic nutrient circulation during the 21st century*, Ch. 4, 51–82 (American Geophysical Union (AGU), 2019).

[5] Munk, W. H. On the wind-driven ocean circulation. *Journal of Meteorology* **7** (2), 80–93 (1950). https://doi.org/10.1175/1520-0469(1950)007⟨0080:OTWDOC⟩2.0.CO;2 .

[6] Buckley, M. W. & Marshall, J. Observations, inferences, and mechanisms of the Atlantic Meridional Overturning Circulation: A review. *Rev. Geophys.* **54** (1), 5–63 (2016). https://doi.org/10.1002/2015RG000493 .

[7] Yang, H. *et al.* Poleward shift of the major ocean gyres detected in a warming climate. *Geophys. Res. Lett.* **47** (5), e2019GL085868 (2020). https://doi.org/10.1029/2019GL085868 .

[8] Wu, L. *et al.* Enhanced warming over the global subtropical western boundary currents. *Nat. Climate Change* **2**, 161–166 (2012). https://doi.org/10.1038/NCLIMATE1353 .

[9] Saba, V. S. *et al.* Enhanced warming of the Northwest Atlantic Ocean under climate change. *J. Geophys. Res.* **121** (1), 118–132 (2016). https://doi.org/10.1002/2015JC011346 .

[10] Jahn, A. E. & Backus, R. H. On the mesopelagic fish faunas of slope water, Gulf Stream, and northern Sargasso Sea. *Deep-Sea Res.* **23** (3), 223–234 (1976). https://doi.org/10.1016/0011-7471(76)91326-7 .

[11] Pershing, A. J. *et al.* Slow adaptation in the face of rapid warming leads to collapse of the Gulf of Maine cod fishery. *Science* **350** (6262), 809–812 (2015). https://doi.org/10.1126/science.aac9819 .

[12] Seo, H. *et al.* Ocean mesoscale and frontal-scale ocean-atmosphere interactions and influence on large-scale climate: A review. *J. Climate* **36** (7), 1981–2013 (2023). https://doi.org/10.1175/JCLI-D-21-0982.1 .

[13] Halkin, D. T. & Rossby, H. T. The structure and transport of the Gulf Stream at 73°W. *J. Phys. Oceanogr.* **15**, 1439–1452 (1985). https://doi.org/10.1175/1520-0485(1985)015⟨1439:TSATOT⟩2.0.CO;2 .

[14] Johns, W. E., Shay, T. J., Bane, J. M. & Watts, D. R. Gulf Stream structure, transport, and recirculation near 68°W. *J. Geophys. Res.* **100** (C1), 817–838 (1995) .

[15] Meinen, C. S. & Luther, D. S. Structure, transport, and vertical coherence of the Gulf Stream from the Straits of Florida to the Southeast Newfoundland Ridge. *Deep-Sea Res. I* **112**, 137–154 (2016). https://doi.org/

10.1016/j.dsr.2016.03.002 .

[16] Webster, F. A description of Gulf Stream meanders off Onslow Bay. *Deep-Sea Res.* **8** (2), 130–143 (1961). https://doi.org/10.1016/0146-6313(61)90005-3 .

[17] Halliwell, G. R., Jr. & Mooers, C. N. K. Meanders of the Gulf Stream downstream from Cape Hatteras 1975–1978. *J. Phys. Oceanogr.* **13** (7), 1275–1292 (1983). https://doi.org/10.1175/1520-0485(1983)013⟨1275:MOTGSD⟩2.0.CO;2 .

[18] Andres, M., Donohue, K. A. & Toole, J. M. The Gulf Stream's path and time-averaged velocity structure and transport at 68.5°W and 70.3°W. *Deep-Sea Res. I* **156**, 103179 (2020). https://doi.org/10.1016/j.dsr.2019.103179 .

[19] Chi, L., Wolfe, C. L. P. & Hameed, S. Has the Gulf Stream slowed or shifted in the altimetry era? *Geophys. Res. Lett.* **48** (14), e2021GL093113 (2021). https://doi.org/10.1029/2021GL093113 .

[20] Yang, H. *et al.* Intensification and poleward shift of subtropical western boundary currents in a warming climate. *J. Geophys. Res.* **121** (7), 4928–4945 (2016). https://doi.org/10.1002/2015JC011513 .

[21] Caesar, L., Rahmstorf, S., Robinson, A., Feulner, G. & Saba, V. Observed fingerprint of a weakening Atlantic Ocean overturning circulation. *Nature* **556**, 191–196 (2018). https://doi.org/10.1038/s41586-018-0006-5 .

[22] Seidov, D., Mishonov, A., Reagan, J. & Parsons, R. Resilience of the Gulf Stream path on decadal and longer timescales. *Sci. Rep.* **9**, 11549 (2019). https://doi.org/10.1038/s41598-019-48011-9 .

[23] Gonçalves Neto, A., Langan, J. A. & Palter, J. B. Changes in the Gulf Stream preceded rapid warming of the Northwest Atlantic Shelf. *Communications Earth and Environment* **2** (74) (2021). https://doi.org/10.1038/s43247-021-00143-5 .

[24] Bisagni, J. J., Gangopadhyay, A. & Sanchez-Franks, A. Secular change and inter-annual variability of the Gulf Stream position, 1993–2013, 70 °–55 °W. *Deep-Sea Res. I* **25**, 1–10 (2017). https://doi.org/10.1016/j.dsr.2017.04.001 .

[25] Dong, S., Baringer, M. O. & Goni, G. J. Slow Down of the Gulf Stream during 1993–2016. *Sci. Rep.* **9** (6672) (2019). https://doi.org/10.1038/s41598-019-42820-8 .

[26] Johnson, G. C. *et al.* Argo–Two decades: Global oceanography, revolutionized. *Annu. Rev. Mar. Sci.* **14**, 379–403 (2022). https://doi.org/10.1146/annurev-marine-022521-102008 .

[27] Riser, S. C. *et al.* Fifteen years of ocean observations with the global Argo array. *Nat. Climate Change* **6**, 145–153 (2016). https://doi.org/10.1038/NCLIMATE2872 .

[28] Sherman, J., Davis, R. E., Owens, W. B. & Valdes, J. The autonomous underwater glider "Spray". *IEEE J. Oceanic Eng.* **26** (4), 437–446 (2001). https://doi.org/10.1109/48.972076 .

[29] Heiderich, J. & Todd, R. E. Along-stream evolution of Gulf Stream volume transport. *J. Phys. Oceanogr.* **50** (8), 2251–2270 (2020). https://doi.org/10.1175/JPO-D-19-0303.1 .

[30] Todd, R. E. Gulf Stream mean and eddy kinetic energy: Three-dimensional estimates from underwater glider observations. *Geophys. Res. Lett.* **48** (6), e2020GL090281 (2021). https://doi.org/10.1029/2020GL090281 .

[31] Chen, Z. *et al.* Long-term SST variability on the northwest Atlantic continental shelf and slope. *Geophys. Res. Lett.* **47** (1), e2019GL085455 (2020). https://doi.org/10.1029/2019GL085455 .

[32] Roemmich, D. *et al.* Unabated planetary warming and its ocean structure since 2006. *Nat. Climate Change* **5**, 240–245 (2015). https://doi.org/10.1038/nclimate2513 .

[33] Forsyth, J. S. T., Andres, M. & Gawarkiewicz, G. G. Recent accelerated warming of the continental shelf off New Jersey: Observations from the CMV Oleander expendable bathythermograph line. *J. Geophys. Res.* **120** (3), 2370–2384 (2015). https://doi.org/10.1002/2014JC010516 .

[34] Le Bras, I. A., Yashayaev, I. & Toole, J. M. Tracking Labrador Sea Water property signals along the Deep Western Boundary Current. *J. Geophys. Res.* **122**, 5348–5366 (2017). https://doi.org/10.1002/2017JC012921 .

[35] Johnson, G. C., Lyman, J. M. & Loeb, N. G. Improving estimates of Earth's energy imbalance. *Nat. Climate Change* **6**, 639–640 (2016). https://doi.org/10.1038/nclimate3043 .

[36] Levitus, S. *et al.* World ocean heat content and thermosteric sea level change (0–2000 m), 1955–2010. *Geophys. Res. Lett.* **39**, L10603 (2012). https://doi.org/10.1029/2012GL051106 .

[37] Bates, N. R. Multi-decadal uptake of carbon dioxide into subtropical mode water of the North Atlantic Ocean. *Biogeosciences* **9**, 2649–2659 (2012). https://doi.org/10.5194/bg-9-2649-2012 .

[38] Li, G. *et al.* Increasing ocean stratification over the past half-century. *Nat. Climate Change* **10**, 1116–1123 (2020). https://doi.org/10.1038/s41558-020-00918-2 .

[39] Sallée, J.-B. *et al.* Summertime increases in upper-ocean stratification and mixed-layer depth. *Nature* **591**, 592–598 (2021). https://doi.org/10.1038/s41586-021-03303-x .

[40] Lee, T. & Cornillon, P. Propagation and growth of Gulf Stream meanders between 75° and 45°W. *J. Phys. Oceanogr.* **26** (2), 225–241 (1996). https://doi.org/10.1175/1520-0485(1996)026⟨0225:PAGOGS⟩2.0.CO;2 .

[41] Gawarkiewicz, G. G., Todd, R. E., Plueddemann, A. J., Andres, M. & Manning, J. P. Direct interaction between the Gulf Stream and the shelf-break south of New England. *Sci. Rep.* **2** (553) (2012). https://doi.org/10.1038/srep00553 .

[42] Andres, M. On the recent destabilization of the Gulf Stream path downstream of Cape Hatteras. *Geophys. Res. Lett.* **43** (18), 9836–9842 (2016). https://doi.org/10.1002/2016GL069966 .

[43] Seidov, D., Mishonov, A. & Parsons, R. Recent warming and decadal variability of Gulf of Maine and Slope Water. *Limnol. Oceanogr.* **66** (9), 3472–3488 (2021). https://doi.org/10.1002/lno.11892 .

[44] Harden, B., Gawarkiewicz, G. G. & Infante, M. Trends in physical properties at the southern New England shelf break. *J. Geophys. Res.* **125**,

e2019JC015784 (2020). https://doi.org/10.1029/2019JC015784 .

[45] Kwon, Y.-O. & Joyce, T. M. Northern hemisphere winter atmospheric transient eddy heat fluxes adn the Gulf Stream and Kuroshio-Oyashio Extenstion variability. *J. Climate* **26** (24), 9839–9859 (2013). https://doi.org/10.1175/JCLI-D-12-00647.1 .

[46] Seo, H., Kwon, Y.-O., Joyce, T. M. & Ummenhofer, C. C. On the predominant nonlinear response of the extratropical atmosphere to meridional shifts of the Gulf Stream. *J. Climate* **30** (23), 9679–9702 (2017). https://doi.org/10.1175/JCLI-D-16-0707.1 .

[47] Johns, E., Watts, D. R. & Rossby, H. T. A test of geostrophy in the Gulf Stream. *J. Geophys. Res.* **94** (C3), 3211–3222 (1989). https://doi.org/10.1029/JC094iC03p03211 .

Methods

In situ observations

This analysis relies on temperature and salinity observations collected by Spray underwater gliders [28] as well as by profiling floats operating as part of the global Argo program [26, 27][48]. Observations from our group's Spray glider surveys in and near the Gulf Stream are publicly available [49, 50]. Argo observations included in the 9 July 2023 snapshot of the Argo Global Data Assembly Center [51] were used. All profiles were averaged into uniform 10-m depth bins with pre-existing quality control flags used to exclude bad data; no further quality control was performed for this analysis. Surface-referenced potential temperature and potential density were calculated using standard algorithms [52]. The temperature and salinity observations come from many distinct conductivity-temperature-depth instruments on the various platforms. As a measure of the cross-instrument precision, all profiles from Argo and gliders were interpolated to a uniform 0.1 kg m^{-3} grid in potential density and the standard deviations of potential temperature and salinity computed on each isopycnal level. The minima in these standard deviations were 0.17 °C and 0.028, respectively, on the 27.5 kg m^{-3} isopycnal, which has a single well-defined water type in the study region. The inferred precision in measurements of potential density is 0.041 kg m^{-3}. It is reasonable to expect that the observations are capable of capturing changes in temperature, salinity, and density that are larger than these values.

Estimation of mean and annual cycle

We used a weighted least-squares approach to estimate the means and annual cycles of temperature, salinity, and velocity in the Gulf Stream region from glider observations. Following the technique previously used to estimate mean velocities from glider-based observations [30], we used a Gaussian weight function with anisotropic and inhomogeneous length scales to account for both ocean circulation and sampling density. Spray glider observations [49, 50] from 52 missions beginning on or after 16 July 2015 and concluding by 30 May 2023 (indicated by the shaded interval in Fig. 1d) were used to estimate the means and annual cycles. The least-squares method for fitting the mean and its local gradient was adapted from [30] to additionally include fitting of the first two harmonics of the annual cycle following [53]; fitting of a third harmonic led to over-fitting of the observations. The resulting 7-parameter fit was of the form

$$\underbrace{\langle d\rangle}_{\text{mean}} + \underbrace{\frac{\partial\langle d\rangle}{\partial r}\Delta r + \frac{\partial\langle d\rangle}{\partial s}\Delta s}_{\text{gradient}} + \underbrace{A_1\sin(t) + B_1\cos(t)}_{\text{annual harmonic}} + \underbrace{A_2\sin(2t) + B_2\cos(2t)}_{\text{semiannual harmonic}}, \tag{1}$$

where $\langle d\rangle$ is the mean of the property d of interest (e.g., temperature, salinity, or velocity); Δr and Δs are distances in the along-mean-flow (r-) and cross-mean-flow (s-) directions between observations and the estimation location; and t is time of year in radians. In determining the length scales at each point and deciding where to mask the resulting estimates of the mean and annual cycle, the criterion for number of seasons sampled from [30] was replaced with a criterion of longest portion of the year not sampled in any year; the threshold for this criterion was 1/6 of the year when used to iteratively determine length scales and 1/4 of the year when used to mask the result. Means and annual cycles were estimated on a $0.1^\circ \times 0.1^\circ$ grid at each 10-m depth level of the vertically binned glider observations and (via linear interpolation of those profiles) on isopycnals spaced by 0.1 kg m^{-3}. Additionally, means and annual cycles were computed on a 5-km$\times$10-km grid in the cross- and along-stream directions at each depth level; this streamwise estimate was produced by assigning each observation location a cross-stream distance relative to the contemporaneous location of the 0.4-m absolute dynamic topography (ADT) contour in the daily SSalto/DUACS gridded altimetry product [54, 55] and an along-stream distance measured along the time-averaged 0.4-m ADT contour. Means and annual cycles of potential temperature and potential density were computed from the fitted means and annual cycles of temperature and salinity.

To estimate standard errors in our fitted annual cycle, we follow [30] to derive the model covariance matrix as a function of the variance in the data and the generalized inverse used in the least squares solution for the annual cycle (see Eq. 9 of the online supplement to [30]). We take the data variance (σ_d^2 in [30]) to be the weighted, squared misfit between observations and the fitted annual cycle. The annual cycle at any time of year is a linear function of the model parameters (i.e., the mean and amplitudes of the annual harmonics), so it is straightforward to estimate the error in the annual cycle for any day of year given the model covariance matrix (e.g., [56]). We take the maximum of this value over the year as a conservative estimate of the standard error in the annual cycle at each grid point and for each variable of interest. Across the three-dimensional grid, the distributions of these uncertainties are positively skewed. For temperature, the mean (median) standard error in the annual cycle in geographic coordinates on depth surfaces is 0.23 (0.19) °C. For salinity, the corresponding mean (median) standard error is 0.03 (0.02). Standard errors in streamwise coordinates on depth surfaces are similar. Standard errors in geographic coordinates on isopycnal surfaces are notably smaller (0.11 (0.04) °C for temperature and 0.03 (0.01) for salinity). Standard errors in the annual cycles of potential temperature are taken to be the same as for temperature. Standard errors for potential density are derived by propagating standard errors on temperature and salinity annual cycles through a local linearization of the equation of state of seawater.

Anomalies and trend estimates

Anomalies relative to the 2015–2023 annual cycle (e.g., Fig. 2) were computed by interpolating the mean and annual cycle to the location and time of year of each (bin-averaged) glider or Argo observation. Isopycnal anomalies are reported at the depth of each underlying (bin-averaged) observation. These interpolations lead to minor errors as evidenced by the isopycnal trends in temperature and salinity not being perfectly compensated in their effect on density (Fig. 3c, red). Anomalies are the difference between observations and fitted annual cycles, both of which have errors defined above; squared errors of anomalies are taken to be the sum of the squared observation precision estimates and the squared standard error in the annual cycle at each location.

Temporal trends (Figs. 2 and 3) were estimated via standard least-squares fitting of anomalies to a linear function of time. Standard errors on the fitted trends were computed with standard techniques of linear estimation [30][56]. We take the data variance to be the sum of squared residuals from the fitted trend plus the squared errors on the anomalies. Autocorrelation in the tightly spaced observations from individual glider missions is accounted for by including off-diagonal elements in the data covariance matrix [56], which we model as a Gaussian function with an e-folding scale that increases linearly from 1.4 days at a depth of 10 m to 3 days at a depth of 1000 m based on fits to empirical autocorrelations of the glider observations; off-diagonal elements corresponding to autocorrelations less than 0.1 are set to zero for numerical convenience. Argo profiles are assumed to be independent. Confidence intervals about fitted trends assume a Student's t-distribution with $n-2$ degrees of freedom and n the number of fitted anomalies, which was typically $O(10^4)$. Due to varying depth resolution of Argo profiles, trends are only reported for depths at which 75% of Argo profiles had data. The 'non-isopycnal' trend at a given depth (green in Fig. 3) was computed by subtracting the trend in properties along isopycnals from the total trend; the error in the resulting estimate was taken to be the square root of the sum of squared errors in the total and isopycnal errors.

Estimates of heat gain

We estimate the rate of heat gain in the upper ocean by vertically integrating the along-isopycnal potential temperature trend $\left\langle \frac{\partial\theta}{\partial t}\Big|_\sigma \right\rangle$ estimated from glider and Argo anomalies (Fig. 3a, red). The shallowest estimate (30 m) is used to fill to the surface. The rate of heat gain $\frac{dQ}{dt}$ above a depth H is

$$\frac{dQ}{dt} = \rho c_p \int_0^H \left\langle \frac{\partial\theta}{\partial t}\bigg|_\sigma \right\rangle dz, \tag{2}$$

where $c_p = 3{,}850$ J °C^{-1} kg^{-1} and $\rho = 1{,}025$ kg m^{-3} are taken as constants following [57]. Integration is performed using a trapezoid rule. We estimate the 95% confidence interval on $\frac{dQ}{dt}$ by propagating uncertainty in the profile of temperature trend (Fig. 3a, red whiskers) under the conservative assumption that those errors are perfectly correlated across depths and using standard error propagation for linear combinations of random variables.

Estimate of Gulf Stream translation rate

The potential density σ of seawater is a function of only the potential temperature θ, the salinity S, and the reference pressure [58] (taken to be zero at the surface here). A change in temperature and salinity at a fixed location in the ocean results from 1) a change in temperature and salinity on a stationary isopycnal (i.e., a change in spice [59]) and/or 2) a vertical or horizontal shift in temperature, salinity, and density fields. We may write

$$\frac{d\theta}{dt} = \left.\frac{\partial\theta}{\partial t}\right|_\sigma - \vec{u}_H \cdot \nabla_H \theta - w\frac{\partial\theta}{\partial z}, \tag{3}$$

$$\frac{dS}{dt} = \left.\frac{\partial S}{\partial t}\right|_\sigma - \vec{u}_H \cdot \nabla_H S - w\frac{\partial S}{\partial z}, \tag{4}$$

$$\frac{d\sigma}{dt} = -\vec{u}_H \cdot \nabla_H \sigma - w\frac{\partial\sigma}{\partial z}, \tag{5}$$

where $\frac{d}{dt}$ denotes the total observed trend, $\left.\frac{\partial}{\partial t}\right|_\sigma$ is the along-isopycnal trend, and $\vec{u}_H = (u, v)$ and w are horizontal and vertical velocities of the temperature, salinity, and density fields. We take the positive x-direction to be directed offshore (equatorward) relative to the Gulf Stream's flow.

To estimate the bulk translation rate of the Gulf Stream, we assumed that lateral and vertical gradients of potential temperature, salinity, and potential density in streamwise coordinates do not vary in time and that motions of the streamwise-averaged fields are spatially uniform and only in the vertical and cross-stream directions (i.e., $v = 0$). Letting $\langle\cdot\rangle$ denote spatial averaging over the Gulf Stream region (Fig. 1a), we then have

$$\left\langle\frac{d\theta}{dt}\right\rangle - \left\langle\left.\frac{\partial\theta}{\partial t}\right|_\sigma\right\rangle = -u\left\langle\frac{\partial\theta}{\partial x}\right\rangle - w\left\langle\frac{\partial\theta}{\partial z}\right\rangle \tag{6}$$

$$\left\langle\frac{dS}{dt}\right\rangle - \left\langle\left.\frac{\partial S}{\partial t}\right|_\sigma\right\rangle = -u\left\langle\frac{\partial S}{\partial x}\right\rangle - w\left\langle\frac{\partial S}{\partial z}\right\rangle \tag{7}$$

$$\left\langle\frac{d\sigma}{dt}\right\rangle = -u\left\langle\frac{\partial\sigma}{\partial x}\right\rangle - w\left\langle\frac{\partial\sigma}{\partial z}\right\rangle. \tag{8}$$

Trends on the left-hand sides of Eqs. (6)–(8) are shown in Fig. 3c–e. Cross-stream and vertical property gradients on the right-hand sides of Eqs. (6)–(8) were obtained as central differences of the streamwise mean fields, neglecting seasonality. Those gradients were then averaged laterally over the Gulf Stream region with standard errors computed in the usual fashion.

Eqs. (6)–(8) may be written in matrix form as

$$\underbrace{\begin{pmatrix} \left\langle \frac{d\theta}{dt} \right\rangle - \left\langle \frac{\partial\theta}{\partial t}\Big|_{\sigma} \right\rangle \\ \left\langle \frac{dS}{dt} \right\rangle - \left\langle \frac{\partial S}{\partial t}\Big|_{\sigma} \right\rangle \\ \left\langle \frac{d\sigma}{dt} \right\rangle \end{pmatrix}}_{\mathbf{d}} \cong \underbrace{\begin{pmatrix} -\left\langle \frac{\partial\theta}{\partial x} \right\rangle & -\left\langle \frac{\partial\theta}{\partial z} \right\rangle \\ -\left\langle \frac{\partial S}{\partial x} \right\rangle & -\left\langle \frac{\partial S}{\partial z} \right\rangle \\ -\left\langle \frac{\partial\sigma}{\partial x} \right\rangle & -\left\langle \frac{\partial\sigma}{\partial z} \right\rangle \end{pmatrix}}_{\mathbf{G}} \begin{pmatrix} u \\ w \end{pmatrix}. \tag{9}$$

Noting that all terms angle brackets are vertical profiles, the dimensions of matrices $\mathbf{d}$ and $\mathbf{G}$ are $(N_\theta + N_S + N_\sigma) \times 1$ and $(N_\theta + N_S + N_\sigma) \times 2$, where $N_\theta = N_S = 32$ and $N_\sigma = 33$ are the number of depth levels at which trends were calculated for each variable; isopycnal trends in temperature and salinity are computed on one less level since some shallow isopycnals outcrop during the year. This system of equations is overdetermined and the weighted least-squares solution for the translation speeds is

$$\begin{pmatrix} u \\ w \end{pmatrix} = \left(\mathbf{G}^\mathsf{T}\mathbf{W}\mathbf{G}\right)^{-1} \mathbf{G}^\mathsf{T}\mathbf{W}\mathbf{d}, \tag{10}$$

where $\mathbf{W}$ is a diagonal weight matrix. We choose to weight equations based on the vertical spacing between trend estimates, which is larger at depth due to varying resolution of some Argo profiles; this yields an estimate of $(u, w)^\mathsf{T}$ that is approximately uniformly weighted over the upper 890 m of the water column. Weighting each equation equally, which biases the estimate toward the surface, yields similar estimates of the bulk motion of the Gulf Stream.

Since terms in both $\mathbf{d}$ and $\mathbf{G}$ have errors, we estimated the resulting errors in u and w via Monte Carlo simulation. The least-squares problem was solved 10,000 times with random fluctuations added to terms in $\mathbf{d}$ and $\mathbf{G}$ drawn from normal distributions with zero mean and standard deviation equal to the corresponding standard errors of the terms. Estimates of u and w are reported as the 95% confidence intervals for the means of the resulting distributions.

Data availability. Data Availability Statement: Spray glider observations used here are available as NetCDF files [49, 50]. Argo data used here are available from [51]. Three-dimensional mean and annual cycle fields derived from glider observations are available as NetCDF files [60]. Plotting makes use of bathymetry from [61] and routines from [62, 63].

Code availability. Matlab code used to estimate trends in Gulf Stream properties is available on Zenodo [64].

Methods-only references

[48] Jayne, S. R. *et al.* The Argo program: Present and future. *Oceanography* **30** (2), 18–28 (2017). https://doi.org/10.5670/oceanog.2017.213 .

[49] Todd, R. E. & Owens, W. B. Gliders in the Gulf Stream [Data set] (2016). https://doi.org/10.21238/S8SPRAY2675.

[50] Todd, R. E. Spray glider observations in support of PEACH [Data set] (2020). https://doi.org/10.21238/S8SPRAY0880.

[51] Argo. Argo float data and metadata from Global Data Assembly Centre (Argo GDAC) - Snapshot of Argo GDAC of July 09st 2023. SEANOE (2023). https://doi.org/10.17882/42182#103614.

[52] Fofonoff, N. P. Physical properties of seawater: A new salinity scale and equation of state for seawater. *J. Geophys. Res.* **90** (C2), 3332–3342 (1985). https://doi.org/10.1029/JC090iC02p03332 .

[53] Rudnick, D. L., Zaba, K. D., Todd, R. E. & Davis, R. E. A climatology of the California Current System from a network of underwater gliders. *Prog. Oceanogr.* **154**, 64–106 (2017). https://doi.org/10.1016/j.pocean.2017.03.002 .

[54] SSALTO/DUACS. Global ocean gridded L4 sea surface heights and derived variables reprocessed 1993 ongoing. https://doi.org/10.48670/moi-00148.

[55] SSALTO/DUACS. Global ocean gridded L4 sea surface heights and derived variables Nrt. https://doi.org/10.48670/moi-00149.

[56] Tellinghuisen, J. Statistical error propagation. *J. Phys. Chem. A* **105**, 3917–3921 (2001). https://doi.org/10.1021/jp003484u .

[57] Talley, L. D., Pickard, G. L., Emery, W. J. & Swift, J. H. *Descriptive Physical Oceanography: An Introduction* Sixth edn (Academic Press, 2011).

[58] Gill, A. E. *Atmosphere-Ocean Dynamics* Vol. 30 of *International Geophysics Series* (Academic Press, San Diego, Calif, 1982).

[59] Munk, W. in *Internal Waves and Small-Scale Processes* (eds Warren, B. & Wunsch, C.) *Evolution of Physical Oceanography–Scientific Surveys in Honor of Henry Stommel* Ch. 9, 264–291 (Mass. Inst. of Technol., Boston, 1981).

[60] Todd, R. E. & Ren, A. S. Gulf Stream mean and annual cycle from Spray underwater glider measurements [Data set] (2023). https://doi.org/10.21238/S8TC9W.

[61] Smith, W. & Sandwell, D. Global seafloor topography from satellite altimetry and ship depth soundings. *Science* **277**, 1957–1962 (1997) .

[62] Thyng, K. M., Greene, C. A., Hetland, R. D., Zimmerle, H. M. & DiMarco, S. F. True colors of oceanography: Guidelines for effective and accurate colormap selection. *Oceanography* **29** (3), 9–13 (2016). https://doi.org/10.5670/oceanog.2016.66 .

[63] Pawlowicz, R. M_Map: A mapping package for MATLAB, v1.4m (2020). URL www.eoas.ubc.ca/~rich/map.html.

[64] Todd, R. E. Matlab code for computing Gulf Stream trends in Todd & Ren (2023, Nature Climate Change). Zenodo (2023). https://doi.org/10.5281/zenodo.8298169.